FINNISH METEOROLOGICAL INSTITUTE
CONTRIBUTIONS

NO. 61

EXPLOITING GROUND-BASED MEASUREMENTS OF THE GLOBAL POSITIONING SYSTEM FOR NUMERICAL WEATHER PREDICTION

Reima Eresmaa

Department of Physical Sciences
Faculty of Science
University of Helsinki
Helsinki, Finland

ACADEMIC DISSERTATION in meteorology

To be presented, with the permission of the Faculty of Science of the University of Helsinki, for public criticism in Auditorium Exactum CK112 (Gustaf Hällströmin katu 2b) on November 16th, 2007, at 12 o'clock noon.

Finnish Meteorological Institute
Helsinki, 2007

ISBN 978-951-697-626-9 (paperback)
ISSN 0782-6117
Yliopistopaino
Helsinki, 2007

ISBN 978-952-10-4122-8 (PDF)
http://ethesis.helsinki.fi
Helsinki, 2007

FINNISH METEOROLOGICAL INSTITUTE

Published by Finnish Meteorological Institute

P.O. Box 503
FIN-00101 Helsinki, Finland

Series title, number and report code of publication
Finnish Meteorological Institute
Contributions 61, FMI-CONT-61

Date
September 2007

Author
Reima Eresmaa

Name of project

Commissioned by

Title
Exploiting ground-based measurements of the Global Positioning System for numerical weather prediction

Abstract

Data assimilation provides an initial atmospheric state, called the analysis, for Numerical Weather Prediction (NWP). This analysis consists of pressure, temperature, wind, and humidity on a three-dimensional NWP model grid. Data assimilation blends meteorological observations with the NWP model in a statistically optimal way. The objective of this thesis is to describe methodological development carried out in order to allow data assimilation of ground-based measurements of the Global Positioning System (GPS) into the High Resolution Limited Area Model (HIRLAM) NWP system. Geodetic processing produces observations of tropospheric delay. These observations can be processed either for vertical columns at each GPS receiver station, or for the individual propagation paths of the microwave signals. These alternative processing methods result in Zenith Total Delay (ZTD) and Slant Delay (SD) observations, respectively. ZTD and SD observations are of use in the analysis of atmospheric humidity.

A method is introduced for estimation of the horizontal error covariance of ZTD observations. The method makes use of observation minus model background (OmB) sequences of ZTD and conventional observations. It is demonstrated that the ZTD observation error covariance is relatively large in station separations shorter than 200 km, but non-zero covariances also appear at considerably larger station separations. The relatively low density of radiosonde observing stations limits the ability of the proposed estimation method to resolve the shortest length-scales of error covariance.

SD observations are shown to contain a statistically significant signal on the asymmetry of the atmospheric humidity field. However, the asymmetric component of SD is found to be nearly always smaller than the standard deviation of the SD observation error. SD observation modelling is described in detail, and other issues relating to SD data assimilation are also discussed. These include the determination of error statistics, the tuning of observation quality control and allowing the taking into account of local observation error correlation. The experiments made show that the data assimilation system is able to retrieve the asymmetric information content of hypothetical SD observations at a single receiver station. Moreover, the impact of real SD observations on humidity analysis is comparable to that of other observing systems.

Publishing unit
Finnish Meteorological Institute, Meteorological Research Unit

Classification (UDC)
551.509.313.22
551.509.313.42
528.8

Keywords
atmospheric humidity, data assimilation,
GPS, HIRLAM, remote sensing

ISSN and series title
0782-6117 Finnish Meteorological Institute Contributions

ISBN
978-951-697-626-9 (paperback), 978-952-10-4122-8 (pdf)

Language
English

Pages
95

Price

Sold by
Finnish Meteorological Institute / Library
P.O. Box 503, FIN-00101 Helsinki, Finland

Note

ILMATIETEEN LAITOS

Julkaisija Ilmatieteen laitos

PL 503, 00101 Helsinki

Julkaisun sarja, numero ja raporttikoodi
Finnish Meteorological Institute
Contributions 61, FMI-CONT-61

Julkaisuaika
Syyskuu 2007

Tekijä
Reima Eresmaa

Projektin nimi

Toimeksiantaja

Nimike
Maanpäällisten satelliittipaikannusmittausten hyödyntäminen numeerisessa säänennustuksessa.

Tiivistelmä

Numeerinen sääennuste perustuu ilmakehää kuvaavan yhtälöryhmän aikaintegrointiin tunnetusta alkutilasta eli analyysistä lähtien. Meteorologinen data-assimilaatio tuottaa analyysin yhdistämällä havaintotiedon sääennustusmallitietoon tilastollisesti optimaalisella tavalla. Analyysi sisältää tietoa ilmanpaineesta, lämpötilasta, tuulesta ja vesihöyryn määrästä kolmiulotteisessa mallihilassa. Tässä väitöskirjassa tarkastellaan maanpäällisten satelliittipaikannusmittausten hyödyntämistä meteorologisina havaintoina HIRLAM (High Resolution Limited Area Model) -sääennustusmallissa. Geodeettisten laskentaohjelmistojen avulla satelliittipaikannusmittaukset pystytään jalostamaan troposfääriviivehavainnoiksi, jotka sisältävät tietoa ilmakehän kosteudesta. Viivehavainnot kuvaavat vesihöyryn määrää joko pystysuunnassa kunkin vastaanottimen yläpuolella (zeniittiviive) tai yksittäisillä vinoilla signaalipoluilla (vinoviive), laskentamenetelmästä riippuen.

Zeniittiviiveen havaintovirheen kovarianssin määrittämiseen esitetään menetelmä, joka pohjautuu havainnon ja sen mallivastineen välisen poikkeaman tilastolliseen analysointiin. Menetelmä hyödyntää zeniittiviivehavaintojen lisäksi radioluotaus- ja pintapainehavaintoja. Menetelmää soveltamalla saadut tulokset osoittavat kovarianssin olevan huomattavan suuri, mikäli havaintoasemien välimatka on pienempi kuin 200 km. Myös pidemmillä välimatkoilla kovarianssi on nollasta poikkeava. Radioluotausasemien suhteellisen pienen lukumäärän vuoksi kovarianssin määrittäminen on vaikeaa, mikäli havaintoasemien välimatka on pieni.

Vinoviivehavaintojen osoitetaan sisältävän tietoa ilmakehän vesihöyryjakauman epäsymmetrisyydestä. Havaintojen epäsymmetrinen komponentti on kuitenkin yleensä pienempi kuin havaintovirheelle määritetty keskihajonta. Vinoviivehavaintojen mallinnus kuvataan yksityiskohtaisesti. Väitöskirjassa tarkastellaan myös muita erityisesti vinoviiveiden hyödyntämiseen liittyviä aiheita, kuten havainto- ja ennustusvirheiden tilastollisten ominaisuuksien määrittämistä, havaintojen laadunvalvontaa ja paikallisen virhekorrelaation huomioonottamista. Suoritetut mallikokeet osoittavat, että vinoviivehavaintojen sisältämä tieto kosteuskentän epäsymmetrisyydestä pystytään hyödyntämään data-assimilaatiojärjestelmän avulla. Vinoviivehavaintojen vaikutus ilmakehän kosteusanalyysiin on realistinen.

Julkaisijayksikkö
Meteorologinen tutkimus

Luokitus (UDK)
551.509.313.22
551.509.313.42
528.8

Asiasanat
data-assimilaatio, GPS, HIRLAM, ilmakehän kosteus, kaukokartoitus

ISSN ja avainnimike
0782-6117 Finnish Meteorological Institute Contributions

ISBN
978-951-697-626-9 (paperback), 978-952-10-4122-8 (pdf)

Kieli
englanti

Sivumäärä
95

Hinta

Myynti
Ilmatieteen laitos / Kirjasto
PL 503, 00101 Helsinki

Lisätietoja

This work is dedicated to *Noora*, *Lyyra* and *Aarni*

PREFACE

The work presented in this thesis has been carried out at the Meteorological research unit of the Finnish Meteorological Institute (FMI) in 2001–2007. I wish to express my gratitude to my supervisor, Prof. Heikki Järvinen, for providing ideas, views and constant support for my work during all these years. I am also grateful to Prof. Hannu Savijärvi, at the University of Helsinki, for his keen interest in my work.

I would like to thank Prof. Mikko Alestalo, Deputy Director of the FMI, for employing me in the numerical weather prediction group of FMI. I would also like to express my gratitude to Section head, Dr. Juhani Damski, for providing support and funding. I thank all of my colleagues in the numerical weather prediction group, in particular group leader Dr. Carl Fortelius, for all their assistance given to my work.

I thank Prof. Markku Poutanen, Finnish Geodetic Institute, and Prof. Jouni Pulliainen, FMI, for reviewing this thesis and for their comments and suggestions towards improving the manuscript.

I wish to thank the co-authors of the Papers included in this thesis for their fruitful co-operation and discussions. I am grateful to my co-operation partners, in particular those involved with the EU FP5 project "Targeting Optimal Use of GPS Humidity measurements in meteorology" and the national project "Geophysically assisted satellite positioning", funded by the Finnish Funding Agency for Technology and Innovation.

Finally, I would like to take this opportunity to thank my exquisite wife Noora and my lovely children Lyyra and Aarni for all the joy they have brought to my life outside working hours.

Helsinki, September 2007

Reima Eresmaa

Contents

LIST OF ORIGINAL PUBLICATIONS

I Eresmaa R. and Järvinen H., (2005): Estimation of spatial GPS Zenith Delay observation error covariance. *Tellus*, **57**A(2), 194–203.

II Eresmaa R. and Järvinen H., (2006): An observation operator for ground-based GPS slant delays. *Tellus*, **58**A(1), 131–140.

III Järvinen H., Eresmaa R., Vedel H., Salonen K., Niemelä S. and de Vries J., (2007): A variational data assimilation system for ground-based GPS slant delays. *Q. J. R. Meteorol. Soc.*, **133**, 969–980.

IV Eresmaa R., Järvinen H., Niemelä S. and Salonen K., (2007): Asymmetricity of ground-based GPS slant delay data. *Atmos. Chem. Phys.*, **7**, 3143–3151.

1 INTRODUCTION

Numerical weather prediction (NWP) models provide the basis for daily weather forecasting. On the scales resolved by the NWP model grid, the atmospheric flow can be characterized by a set of non-linear partial differential equations (e.g. Holton, 1992; Pielke, 2002). The evolution of the pressure, temperature, wind and humidity (water vapour) fields in the model atmosphere follows from time integration of these equations, starting from the best available initial state. The accuracy of the resulting NWP forecast depends on the accuracies of the initial model state, the numerical formulation of the atmospheric dynamics, and the physical parameterization schemes adopted in order to account for the sub-grid scale processes.

The following properties are characteristic of atmospheric water vapour: First, the horizontal and vertical length scales are short compared with those of pressure and temperature (Berre, 2000). Second, the coupling of humidity with other atmospheric quantities is weak. Third, steep horizontal and vertical gradients are common. Fourth, the distribution of the water vapour concentrations actually occurring in the atmosphere is special; concentrations vary rather uniformly between zero and a slight supersaturation. Finally, water vapour plays a key role in several processes of relevance in NWP. These processes include, e.g., cloud and rain formation, the absorption and emission of latent heat, and solar and terrestrial radiative transfer.

As operational NWP systems evolve towards convective-scale modelling, observing systems are needed capable of measuring atmospheric humidity at a high resolution. Traditionally, the radiosonde observing network has been the most important source of humidity information for NWP. This information is supplemented by in situ measurements from synoptic ground stations and aircrafts. Remote sensing technology provides a further increase in the number of available humidity observations. There are two basically different principles used for the remote sensing of water vapour. First, the effect of humidity on atmospheric radiation properties is exploited by measuring the radiation emitted by the atmosphere, either by space-borne or ground-based sensors in the infrared or microwave part of the electromagnetic spectrum (Andersson et al., 1994; Derber and Wu, 1998; Feltz et al., 2003). Second, advantage is taken of the relationship between humidity and microwave refractivity. Such refractivity measurements can be processed, in integrated form, as by-products of geodetic processing using ground-based measurement data from the Global Positioning System (GPS) (Bevis et al., 1992; Elgered et al., 2005). In the context of GPS meteorology, the integrated refractivity measurements are referred to as tropospheric delay observations.

This thesis reviews methodological development carried out in the framework of the High Resolution Limited Area Model (HIRLAM) NWP system in order to allow data assimilation of tropospheric delay observations. The thesis consists of an introductory part and four original publications, which are referred to as Papers I–IV. The introductory part is structured as follows. The framework of NWP and data assim-

ilation is outlined in Chapter 2, followed by a discussion on the ground-based GPS observations in Chapter 3. The main results concerning the data assimilation of the tropospheric delay observations, presented in Papers I–IV, are discussed in Chapter 4. Chapter 5 presents the conclusions.

The contents of Papers I–IV and the author's contribution are briefly outlined below.

I PAPER I presents and illustrates a method for determination of the horizontal error covariance of GPS Zenith Total Delay observations. The method is an extension of the observation method, introduced by Hollingsworth and Lönnberg (1986), to the general case of correlated observation errors. As a result, least-squares-fitted coefficients of a four-parameter covariance function are provided separately for each season and for the yearly mean. The author of this thesis is responsible for all the calculations and for a large part of the analyses and writing.

II PAPER II introduces an algorithm for numerical modelling of GPS Slant Delay (SD) observations. Such an algorithm can be applied as an observation operator in variational data assimilation for NWP. The paper includes an algorithm description and validation against geodetically-processed SD observations. The author has contributed to the observation operator design and is responsible for all coding and experimentation and for a large part of the writing.

III PAPER III describes the implementation of SD data assimilation in the context of the HIRLAM 3D-Var data assimilation system. The implementation covers aspects of the observation operator, the determination of observation and background error statistics, the tuning of background quality control, and the implementation of observation error correlations. The paper also validates the implementation by data assimilation impact studies utilizing hypothetical and real SD observations. The author has contributed to the data assimilation system development, and is responsible for all coding and experimentation, as well as a major part of the writing.

IV PAPER IV investigates the azimuthally asymmetric properties of SD observations and their NWP model counterparts. The contribution of azimuthal asymmetry is found to be usually below the level of measurement noise. Nevertheless, cases of extreme asymmetry are shown to be related to actual atmospheric features. Moreover, the NWP model's representation of the asymmetric information content is shown to improve with increasing horizontal resolution. The author is the primary contributor of the article, including the experiment design, running the HIRLAM NWP model, analysis of the results and writing.

2 NUMERICAL WEATHER PREDICTION

NWP systems can be divided into two groups according to the model domain. *Global* NWP systems cover the whole Earth with a grid spacing of around 20–50 km and provide forecasts up to 10–15 days ahead. *Limited area models* cover smaller geographical areas of interest with a denser grid than that in global models, and provide forecasts up to 48–72 hours ahead. Convective-scale models, which are being developed at present, are limited area models aiming at short-range forecasts up to 3–18 hours ahead. Limited area models require external input for the lateral boundary conditions; usually these input data are retrieved from either coarser resolution limited area model forecasts or from global NWPs.

Deterministic NWP systems consist of two main components, which are the *analysis system* and the *forecast model*. The purpose of the analysis system is to provide the initial condition for the forecast model. In a statistical sense, the optimal initial condition results from the process of data assimilation. The forecast model, on the other hand, integrates the model equations forward in time in order to provide predictions of atmospheric state at a given time in the future. Failure in the performance of either of these components inevitably leads to an unsuccessful numerical forecast.

2.1 DATA ASSIMILATION METHODS

Determination of the initial condition (analysis) for the forecast model is a statistical estimation problem, which is solved by the methods of data assimilation. In short, data assimilation updates the model background field by using the new information contained in meteorological observations. The model background field is usually a short-range forecast from the previous analysis. A statistically optimal data assimilation scheme searches for the maximum-likelihood estimate of the atmospheric state by taking the statistical properties of observation and background errors into account.

Starting from the bayesian probability theory, Lorenc (1986) derived the cost function

$$\begin{aligned} J(\mathbf{x}) &= \frac{1}{2}(\mathbf{x}-\mathbf{x_b})^T\mathbf{B}^{-1}(\mathbf{x}-\mathbf{x_b}) \\ &+ \frac{1}{2}(H[\mathbf{x}]-\mathbf{y})^T\mathbf{R}^{-1}(H[\mathbf{x}]-\mathbf{y}), \end{aligned} \tag{2.1}$$

where $\mathbf{x}$ is the model state, $\mathbf{x_b}$ is the background field, $\mathbf{y}$ represents the observations, $\mathbf{B}$ and $\mathbf{R}$ are the background and observation error covariance matrices, respectively, and H is the observation operator producing the model equivalent to the observations from a given $\mathbf{x}$. Under the assumptions that the observation and background errors are random gaussian with zero mean and uncorrelated with each other, the statistically optimal analysis corresponds to the minimum of the cost function (2.1). The optimal

analysis thus essentially minimizes the squared departures from the background and the observations, weighted by their respective errors.

Variational data assimilation

Variational data assimilation algorithms are based on iterative minimization of the cost function J. It is useful to formulate the cost function by means of an analysis increment $\delta\mathbf{x}$ defined as

$$\delta\mathbf{x} = \mathbf{x} - \mathbf{x_b}. \tag{2.2}$$

Combining Eqs. (2.1) and (2.2) yields

$$\begin{aligned} J(\delta\mathbf{x}) &= \frac{1}{2}\delta\mathbf{x}^T\mathbf{B}^{-1}\delta\mathbf{x} \\ &+ \frac{1}{2}(H[\mathbf{x_b}+\delta\mathbf{x}]-\mathbf{y})^T\mathbf{R}^{-1}(H[\mathbf{x_b}+\delta\mathbf{x}]-\mathbf{y}). \end{aligned} \tag{2.3}$$

In practical NWP applications, the minimization of the cost function is not possible unless the problem is linearized around the background. Introducing the tangent-linear observation operator

$$\mathbf{H} = \left.\frac{\partial H}{\partial \mathbf{x}}\right|_{\mathbf{x}=\mathbf{x_b}}, \tag{2.4}$$

and assuming the validity of the tangent-linear hypothesis[1]

$$H[\mathbf{x_b}+\delta\mathbf{x}] - H[\mathbf{x_b}] = \mathbf{H}\delta\mathbf{x}, \tag{2.5}$$

allows one to write Eq. (2.3) as

$$\begin{aligned} J(\delta\mathbf{x}) &= \frac{1}{2}\delta\mathbf{x}^T\mathbf{B}^{-1}\delta\mathbf{x} \\ &+ \frac{1}{2}(H[\mathbf{x_b}]-\mathbf{y}+\mathbf{H}\delta\mathbf{x})^T\mathbf{R}^{-1}(H[\mathbf{x_b}]-\mathbf{y}+\mathbf{H}\delta\mathbf{x}). \end{aligned} \tag{2.6}$$

Equation (2.6) is known as the incremental cost function (Courtier et al., 1994).

In variational data assimilation algorithms, the analysis control vector is updated by the gradient of the cost function

$$\nabla_{\delta\mathbf{x}} J = \mathbf{B}^{-1}\delta\mathbf{x} + \mathbf{H}^T\mathbf{R}^{-1}(H[\mathbf{x_b}]-\mathbf{y}+\mathbf{H}\delta\mathbf{x}) \tag{2.7}$$

at each iteration step. The transpose of the tangent-linear observation operator ($\mathbf{H}^T$) is often called the adjoint of the observation operator. This adjoint operator transforms the

[1]The tangent-linear hypothesis states that the second- and higher-order terms of a Taylor series expansion are negligible.

weighted departure between the model state and the observations from the observation space to the model space.

Equations (2.1)-(2.7) are general and they can, in principle, be applied to a large variety of problems dealing with the state estimation of a dynamical system. In NWP applications, the variational data assimilation is usually performed in either three (3D-Var) or four (4D-Var) dimensions. The model equivalents to the observations are produced through observation modelling by the observation operator H. In 4D-Var, the observation modelling involves model state integration in time in addition to the three-dimensional observation modelling performed in 3D-Var. This implies that the 4D-Var data assimilation system needs to be supplemented with a dynamical forecast model. The forecast model equations, in addition to the observation operator, are linearized in 4D-Var around the background field. Therefore, tangent-linear and adjoint codes need to be written for the forecast model in a similar fashion as those written for the observation operator.

Alternative data assimilation algorithms

Most of the data assimilation methods currently in use for NWP, including three-dimensional variational data assimilation, are approximations of the Extended Kalman Filter (EKF)[2]. EKF is a sequential estimation algorithm, which updates the state estimate *at each time step* using the new observations and an a priori estimate derived from the previous state estimate. In addition to the state estimate, the full EKF updates the error covariance matrix for the state estimate at each time step. Moreover, both the state estimate and the error covariance matrix are propagated forward to the next time step in such a way that the error covariances of the forecast model are taken into account. While the Kalman filter has proved to be very useful for the state estimation of dynamical systems of a limited dimension, it is too expensive to be used for meteorological data assimilation.

Variational data assimilation uses iterative methods in order to find the minimum of the cost function. In low-dimension analysis problems, the cost function minimum can also be solved explicitly by setting the cost function gradient (2.7) to zero and solving the resulting equation for $\delta\mathbf{x}$. This approach yields a minimum-variance estimate of $\mathbf{x}$ with no assumptions about the observation or background error probability distribution functions. The formerly popular data assimilation algorithm of Optimum Interpolation (OI) uses this approach. The increasing need for the use of remote sensing based observations limits the usability of the OI algorithm.

The Ensemble Kalman Filter (EnKF; Evensen, 1994) is widely considered as one of the most relevant approximations of EKF from the modern NWP point of view. While the full EKF provides the analysis error covariance matrix explicitly, EnKF ap-

[2]Four-dimensional variational data assimilation is an approximation of the Kalman Smoother, which is a generalization of EKF.

proximates this matrix on the basis of a spread between a number of equally likely state estimates. Ensemble sizes of around 100 are found to be operationally feasible and still large enough for NWP applications (Houtekamer and Mitchell, 2001). However, approximations like EnKF have not, so far, shown improved skill over the variational data assimilation algorithms.

2.2 MODEL DYNAMICS AND PHYSICAL PARAMETERIZATIONS

The deterministic propagation of the NWP model state in time is governed by the following partial differential equations (e.g. Pielke, 2002):

$$\frac{\partial \vec{V}}{\partial t} = -\vec{V} \cdot \nabla \vec{V} - 2\vec{\Omega} \times \vec{V} - \rho^{-1} \nabla p + \vec{g} \tag{2.8}$$

$$\frac{\partial \rho}{\partial t} = -(\nabla \cdot \rho \vec{V}) \tag{2.9}$$

$$\frac{\partial \theta}{\partial t} = -\vec{V} \cdot \nabla \theta + S_\theta \tag{2.10}$$

$$\frac{\partial q_n}{\partial t} = -\vec{V} \cdot \nabla q_n + S_{q_n}, \qquad n = 1, 2, 3 \tag{2.11}$$

$$\frac{\partial \chi_m}{\partial t} = -\vec{V} \cdot \nabla \chi_m + S_{\chi_m}, \qquad m = 1, 2, \ldots, M \tag{2.12}$$

This set of partial differential equations represents the physical conservation laws of momentum, mass, heat, water, and other gaseous constituents of air, respectively. In Eqs. (2.8)-(2.12), t is the time, $\vec{V}$ is the wind vector, ρ is the density, θ is the potential temperature, q_n is the mass ratio between each of the water phases and air, and χ_m is the mass ratio between any chemical substance and air. Moreover, $\vec{\Omega}$ is the angular velocity of the Earth's rotation, p is the pressure, and $\vec{g}$ is the gravitational acceleration. S_θ, S_{q_n}, and S_{χ_m} represent the source / sink terms of heat, water (in any of its three phases) and other chemical constituents, respectively. This set of equations constitutes the NWP model dynamics, and it is solved at each time step of the model integration.

The need for physical parameterizations arises from the numerical discretization of the model dynamics. The NWP model uses grid-box averaging in four dimensions. This means that the atmosphere is approximated as a set of grid boxes, and only the grid box mean values of the atmospheric quantities at each time step are explicitly determined. The decomposition

$$\phi = \overline{\phi} + \phi' \tag{2.13}$$

illustrates this concept. In Eq. (2.13), ϕ represents any one of the variables appearing in Eqs. (2.8)-(2.12). The value of ϕ at any time instant at any single point can be thought of as a sum of the grid box mean value $\overline{\phi}$ and the deviation from the grid box mean, i.e., the subgrid scale perturbation ϕ'. This decomposition is applied to all variables appearing in Eqs. (2.8)-(2.12).

According to the definition, the grid-box averaging of the subgrid scale perturbations results in zero. This simplifies the formulation of the model equations, as most of the actually-needed terms are not contributed to by the subgrid scale perturbation. The net effect of the subgrid scale perturbations felt on the resolvable scale comes from products of the form $\overline{\phi'\phi'}$. This net effect needs to be parameterized as a function of the grid box mean values. The development of physical parameterization methods is an area of active research (e.g. Niemelä and Fortelius, 2005; Rontu, 2006).

3 GROUND-BASED GPS OBSERVING SYSTEM

At the time of writing, the space segment of GPS consists of 31 satellites in circular orbits at a height of about 20 200 km above the ground. Each GPS satellite transmits a modulated signal at two frequencies in the microwave domain. Simultaneous reception of signals from at least four GPS satellites allows determination of the receiver coordinates in the terrestrial reference frame (e.g. Hofmann–Wellenhof et al., 2001; Strang and Borre, 1997). While relatively cheap, portable GPS receivers are able to provide real-time positioning accuracy as high as a few metres by utilizing so-called code pseudorange measurements, the receivers used for geophysical research can provide absolute accuracy of a few centimetres. Such an increased positioning accuracy is achieved by geodetic post-processing of dual-frequency measurements of so-called phase pseudoranges over a time interval of considerable duration. Figure 3.1 shows the positions of the Global Positioning System (GPS) satellites as viewed at the permanent receiver station Oulu, maintained by the Finnish Geodetic Institute (FGI), on 1 October 2005 at 00–01 UTC.

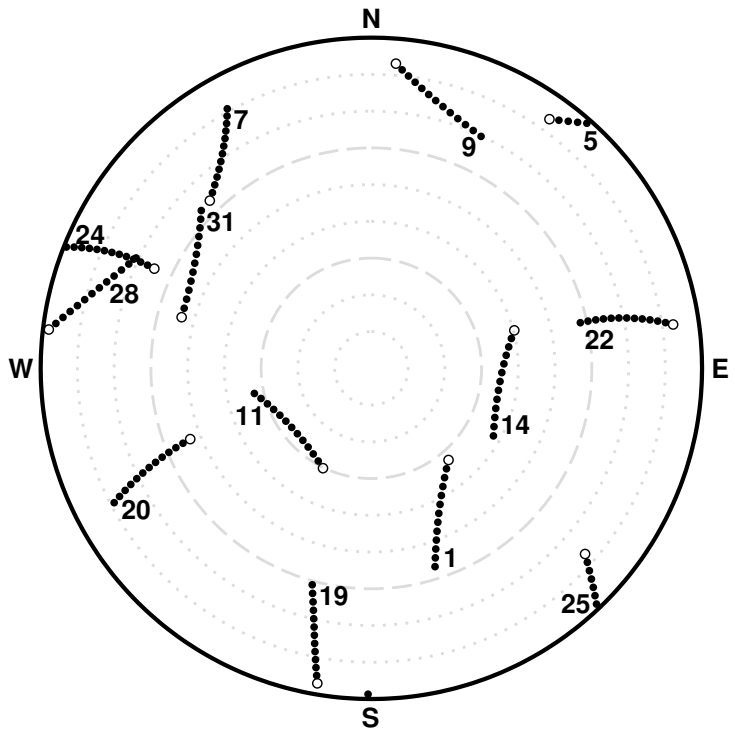

FIGURE 3.1. Positions of the GPS satellites in the sky as viewed at the Oulu GPS receiver station on 1 October 2005 at 00–01 UTC. Circles denote the positions of each satellite at 01 UTC. The northern (eastern) horizon is on top (right) and the zenith is in the middle.

3.1 TROPOSPHERIC DELAY

The atmospheric effect on GPS signal propagation rises from ionized particles on the one hand, and from the neutral medium on the other. These two phenomena are known as ionospheric delay and tropospheric delay, respectively. Ionospheric delay is dispersive and depends on the frequency of the microwave signal. Dual-frequency measurements thus allow one to a large extent to eliminate the ionospheric delay in processing. Taking the ionospheric (Δ^I) and tropospheric (Δ^T) delays into account, the phase pseudorange observation equation can be written as (Blewitt, 1997)

$$L = \varrho + c(\delta_{rec} - \delta^{sat}) + \lambda(\varphi_{0,rec} - \varphi_0^{sat}) - \lambda N_i + \Delta^T - \Delta^I, \tag{3.1}$$

where L is the phase pseudorange, i.e., the phase difference, in length units, between the received carrier wave and the referencing wave created by the receiver, ϱ is the distance between the satellite and the receiver, c is the vacuum speed of light, δ_{rec} and δ^{sat} are the clock biases of the receiver and the satellite, respectively, λ is the wavelength of the carrier wave, $\varphi_{0,rec}$ and φ_0^{sat} are the initial phases of the referencing wave and the carrier wave, respectively, and N_i is the integer ambiquity, i.e., the number of full wavelengths between the satellite and the receiver.

The tropospheric delay is defined as the difference between (i) the real travel time of a signal from a GPS satellite to a ground-based receiver and (ii) the travel time that would occur if there was no atmosphere affecting the signal propagation. In practical applications, tropospheric delay is usually expressed as the time difference multiplied by the vacuum speed of light. This allows one to interpret the tropospheric delay as the apparent excess path length due to the neutral atmosphere. The contribution of tropospheric delay to a pseudorange measurement is of the order of 2–3 metres, if the satellite is relatively close to local zenith and the receiver is located near the mean sea level.

Formally, the tropospheric delay is written as

$$\Delta^T = \int_s n\, ds - \int_g dg, \tag{3.2}$$

where n is the real part of the atmospheric refractive index, s is the actual signal path through the atmosphere, and g is the geometrical path, i.e., the hypothetical signal path that would occur without the atmospheric effect. It is possible to rewrite Eq. (3.2) as

$$\begin{aligned} \Delta^T &= \int_s n\, ds - \int_g dg \\ &= \int_s (n-1)\, ds + \left(\int_s ds - \int_g dg \right). \end{aligned} \tag{3.3}$$

This expression shows that the tropospheric delay is contributed to by the decrease of the microwave propagation speed on the one hand, and by the increased path length on the other. The latter effect is sometimes called the geometric delay and is of significance

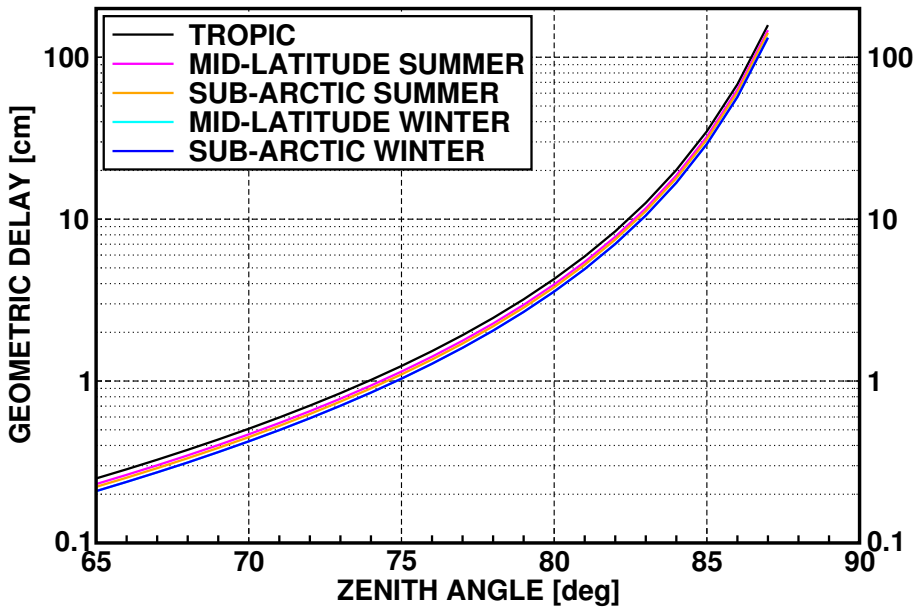

FIGURE 3.2. Increase of the microwave propagation path length (geometric delay) as a function of satellite zenith angle in the reference atmospheres.

when measurements from very large zenith angles (low elevation angles) are concerned. Figure 3.2 shows the contribution of the geometric delay as a function of satellite zenith angle in the reference atmospheres of McClatchey et al. (1971). At a satellite zenith angle of 80°, for instance, the bending term accounts for about 4 cm. At smaller zenith angles, the delay due to the decrease of propagation speed accounts for more than 99.7% of the total tropospheric delay.

The geometric delay is assumed negligible throughout the work presented in this thesis. With this assumption, the tropospheric delay reduces to the integral of refractivity along the signal propagation path s through the atmosphere, i.e.,

$$\Delta^T = \int_s (n-1)ds = 10^{-6}\int_s N ds, \tag{3.4}$$

where N=$10^6(n-1)$ is the refractivity. Moreover, in the microwave range N is related to atmospheric quantities through

$$\begin{aligned} N &= 10^{-6}(n-1) \\ &= k_1\frac{p_d}{T}Z_d^{-1} + k_2\frac{e}{T}Z_w^{-1} + k_3\frac{e}{T^2}Z_w^{-1}, \end{aligned} \tag{3.5}$$

where p_d and e are the pressures of dry air and water vapour, respectively, T is the temperature, Z_d and Z_w are the compressibility factors of dry air and water vapour, respectively and k_1, k_2 and k_3 are coefficients with empirically-determined values. Equations (3.4) and (3.5) provide the basis for the concept known as ground-based GPS meteorology (Bevis et al., 1992).

In the case of a receiver operating over a sufficiently long period of time, the unknown parameters of Eq. (3.1), including Δ^T, can be solved as a least-squares adjustment using the methods of linear algebra. From the perspective of NWP, the GPS data processing needs to be carried out in near-real-time, i.e., within 1–2 hours after signal reception. Several data processing centres in Europe, the United States and Japan have shown that the processing and delivery of tropospheric delay estimates is possible in near-real-time without introducing too large an increase in the noise level of the processing output (Elgered et al., 2005).

3.2 ZENITH DELAY OBSERVATIONS

Most geodetic processing software supports an estimation of the Zenith Total Delay (ZTD) from the raw pseudorange measurements in a network of ground-based GPS receiver stations. ZTD is a measure of the tropospheric delay in the zenith direction at a single receiver station. A significant amount of research has been conducted on the use of processed ZTD observations for NWP applications (e.g. De Pondeca and Zou, 2001; Vedel and Huang, 2004; Elgered et al., 2005). Data assimilation of ZTD observations into limited area NWP systems has recently become operational practice both at Meteo-France and at the UK Met Office, and similar activities are expected to take place in the near future at other meteorological institutes, too.

In GPS data processing, it is usually beneficial to separate ZTD in two components, the Zenith Hydrostatic Delay (ZHD) and the Zenith Wet Delay (ZWD) (Bevis et al., 1992). ZTD is always dominated by ZHD; in typical atmospheric conditions, ZHD accounts for more than 90% of ZTD. While ZHD can be relatively accurately modelled in terms of surface pressure measurements, it is ZWD which has the largest potential for meteorological applications. This follows from the fact that ZWD is sensitive to humidity at higher altitudes, which is not the case with ZHD.

The barometric pressure p can be separated into the partial pressures of dry air (p_d) and water vapour (e). Let us further assume that both dry air and water vapour are ideal gases, i.e., the compressibility factors appearing in Eq. 3.5 are Z_d=Z_w=1.0 (Bevis et al., 1992). Under the ideal gas assumption, the densities of dry air and water vapour (ρ_d and ρ_w) are

$$\rho_d = \frac{p_d}{R_d T}, \text{ and} \tag{3.6}$$

$$\rho_w = \frac{e}{R_w T}, \tag{3.7}$$

where R_d and R_w are the gas constants of dry air and water vapour, respectively. The density of the compound air is simply obtained as a sum

$$\rho = \rho_d + \rho_w. \tag{3.8}$$

The refractivity can then be written as

$$\begin{aligned} N &= k_1\frac{p_d}{T} + k_2\frac{e}{T} + k_3\frac{e}{T^2} \\ &= k_1\rho_d R_d + k_2\rho_w R_w + \frac{k_3\rho_w R_w}{T} \\ &= k_1(\rho-\rho_w)R_d + k_2\rho_w R_w + \frac{k_3\rho_w R_w}{T} \\ &= k_1\rho R_d + (k_2R_w - k_1R_d)\rho_w + \frac{k_3\rho_w R_w}{T}. \end{aligned} \tag{3.9}$$

Since we are dealing with zenith delays, the signal path s is a vertical column, Δ^T is equal to ZTD, and the integration of Eq. 3.4 is performed between the GPS receiver altitude z_r and infinity. Therefore,

$$\begin{aligned} ZTD &= 10^{-6}\int_{z_r}^{\infty} N dz \\ &= 10^{-6}\int_{z_r}^{\infty} k_1\rho R_d dz + 10^{-6}\int_{z_r}^{\infty}(k_2R_w - k_1R_d)\rho_w dz \\ &+ 10^{-6}\int_{z_r}^{\infty}\frac{k_3\rho_w R_w}{T}dz. \end{aligned} \tag{3.10}$$

The first term on the right-hand-side of Eq. (3.10) integrates the density of compound air, including both dry and moist constituents, while the remaining two terms integrate water vapour density and the ratio of water vapour density and temperature, respectively. The first term is interpreted as ZHD. Applying the hydrostatic equation

$$dp = -g\rho dz, \tag{3.11}$$

where g is the local gravitational acceleration, allows one to transform the first term through

$$\begin{aligned} ZHD &= 10^{-6}\int_{z_r}^{\infty} k_1\rho R_d dz = 10^{-6}k_1R_d\int_0^{p_r}\frac{dp}{g} \\ &= 10^{-6}\frac{k_1R_d}{g^*}\int_0^{p_r} dp = 10^{-6}\frac{k_1R_d}{g^*}p_r, \end{aligned} \tag{3.12}$$

where g^* is the local gravitational acceleration at the centre of mass of the vertical air column and the integration is performed between zero and pressure p_r at the receiver level. g^* is about 0.2 ms^{-2} smaller than the local gravitational acceleration at mean sea level. Equation (3.12), shows the dependency of ZHD on receiver level pressure. The dependence of ZWD on the vertical distributions of meteorological quantities is given by the second and third terms of Eq. (3.10), and it cannot be essentially simplified without making additional assumptions.

GPS data processing makes use of prescribed mapping functions for relating a delay component corresponding to a satellite at an arbitrary zenith angle to a zenith delay. In modern GPS meteorology, the most widely-adopted mapping functions are

those suggested by Niell (1996), Niell (2001), Boehm and Schuh (2004) and Boehm et al. (2006). All of these mapping functions are specified separately for the hydrostatic and wet delay contributions. Using the hydrostatic and wet mapping functions (m_h and m_w), the tropospheric refraction can be formulated as

$$\Delta^T = m_h ZHD + m_w ZWD. \tag{3.13}$$

Since ZHD can be determined from the surface measurements of pressure alone, it is ZWD which is usually estimated as a part of the GPS data processing. Finally, the ZTD observation is obtained as a sum of ZHD and ZWD.

Papers I–IV included in this thesis use the values suggested by Bevis et al. (1994) for the refractivity coefficients appearing in Eqs. (3.5), (3.9), (3.10) and (3.12). These values are k_1 = 77.60 K hPa^{-1}, k_2 = 70.4 K hPa^{-1} and k_3 = 3.739$\times 10^{-5}$ K^2 hPa^{-1}. The gas constants for dry air and for water vapour are R_d = 287.04 J kg^{-1} K^{-1} and R_w = 461.50 J kg^{-1} K^{-1}, respectively.

3.3 Integrated Water Vapour observations

By making additional assumptions about the vertical temperature and humidity profiles, the obtained ZTD from the GPS measurements can be further processed into Integrated Water Vapour (IWV). There have been reports on the use of GPS-derived IWV estimates for NWP (Pacione et al., 2001; Falvey and Beavan, 2002; Guerova et al., 2006) or for nowcasting (De Haan et al., 2004).

The IWV in the vertical column above the GPS receiver is

$$IWV = \int_{z_r}^{\infty} \rho_w dz. \tag{3.14}$$

On the other hand, ZWD is

$$\begin{aligned} ZWD &= 10^{-6} \int_{z_r}^{\infty} (k_2 R_w - k_1 R_d) \rho_w dz + 10^{-6} \int_{z_r}^{\infty} \frac{k_3 \rho_w R_w}{T} dz \\ &= 10^{-6} (k_2 R_w - k_1 R_d) \int_{z_r}^{\infty} \rho_w dz + 10^{-6} k_3 R_w \int_{z_r}^{\infty} \frac{\rho_w}{T} dz. \end{aligned} \tag{3.15}$$

In order to derive a relationship between ZWD and IWV, it is useful to introduce a weighted mean temperature of the vertical column as

$$T_m = \frac{\int_{z_r}^{\infty} \rho_w dz}{\int_{z_r}^{\infty} (\rho_w / T) dz}. \tag{3.16}$$

This relation is identical to

$$\int_{z_r}^{\infty} \frac{\rho_w}{T} dz = \frac{\int_{z_r}^{\infty} \rho_w dz}{T_m}, \tag{3.17}$$

and Eq. (3.15) can now be rewritten as

$$\begin{aligned} ZWD &= 10^{-6}(k_2 R_w - k_1 R_d + k_3 \frac{R_w}{T_m}) \int_{z_r}^{\infty} \rho_w dz \\ &= 10^{-6}(k_2 R_w - k_1 R_d + k_3 \frac{R_w}{T_m}) IWV. \end{aligned} \tag{3.18}$$

Conversion of ZWD into IWV thus depends on T_m, which in turn depends on the vertical profiles of temperature and humidity. In practical applications, T_m is determined from the surface measurements by using some kind of regression formula. This procedure is likely to increase IWV observation error variance and introduce horizontal and temporal observation error correlations. For this reason, ZTD observations are usually preferred over IWV observations in the variational data assimilation framework.

3.4 SLANT DELAY OBSERVATIONS

Estimating tropospheric delays along the actual signal paths between GPS satellites and ground-based receiver stations provides Slant Delay (SD) observations. Compared with ZTD observations, SD observations have the following advantages: First, as shown by Eq. (3.4), the tropospheric delay actually occurs along slanted signal paths. Therefore, SD observations represent the observed quantities. Second, applying tomographical methods to SD observations allows the retrieval of the three-dimensional humidity distribution. As ZTD observations are vertical integrals, the best that they can provide is a two-dimensional field of IWV. Third, SD observations contain less filtering. While a ZTD observation represents an averaged measure of tropospheric delay, an SD observation is considered as a line measurement. Fourth, SD observations potentially contain azimuthally asymmetric humidity information. Such information is of significance in regions characterized by atmospheric humidity gradients. These advantages make SD a particularly interesting observation type from the data assimilation point of view.

The inherent characteristic of containing azimuthally asymmetric information is one of the most interesting properties of SD observations. To assess the relevance of this property, it is essential to be able to separate SD observations into azimuthally symmetric and asymmetric components. Traditional GPS data processing, in fact, produces the azimuthally symmetric component SD_s as a linear combination of ZHD and ZWD as given by Eq. (3.13). If SD observations are meant to provide information that is not provided by ZTD observations, it is crucial to be able to retrieve the azimuthally asymmetric component SD_a as a part of the processing.

SD data processing has been discussed by Ware et al. (1997), Alber et al. (2000) and De Haan et al. (2002). All of these studies rely on the assumption that SD_a can be retrieved from fitting residuals of the geodetic least-squares network solution. This means that all such errors affecting the GPS processing, that are not explicitly removed, end up in the processed SD observations. Moreover, since the least-squares method simultaneously adjusts all the unknown parameters to find the optimal fit to all the

measurements, it is unlikely that the actual residuals have a one-to-one correspondence with the actual asymmetric contribution of tropospheric delay in the raw pseudorange measurements. This aspect has been brought up by Elosegui and Davis (2003). It can be summarized that currently-used SD data processing techniques are unsuitable from the NWP point of view, and further research is needed before operational processing of SD observations can be considered reasonable for data assimilation.

Partly due to the unsolved questions concerning SD data processing, the SD data assimilation experiments reported so far have focused on the use of hypothetical SD observations (MacDonald et al., 2002; Ha et al., 2003; Liu and Xue, 2006). All of these studies have shown that the idealized SD observations have the potential to improve the retrieval of the humidity field compared with the data assimilation of ZTD observations. However, it has not yet been shown that the real SD observations have such properties.

4 DEVELOPMENT OF GROUND-BASED GPS DATA ASSIMILATION

This chapter provides an overview of the scientific results originally reported in the papers included in this thesis. All of the results have been obtained in the framework of the three-dimensional data assimilation (3D-Var) system (Gustafsson et al., 2001; Lindskog et al., 2001) of the High Resolution Limited Area Model (HIRLAM; Undén et al., 2002). The results presented in Papers I, II, III, and IV are discussed in Sections 4.1, 4.2, 4.3, and 4.4, respectively.

4.1 ZTD OBSERVATION ERROR COVARIANCE

The errors of two independent observations are uncorrelated with each other. For example, two separate barometers provide independent pressure measurements, and the corresponding observation errors are uncorrelated. In contrast, mutually-dependent observations imply correlated observation errors. There are two cases that result in mutually-dependent observations. First, if several observations originate from a single observing instrument, for instance from a radiosonde sensor or a doppler radar, the observations are mutually dependent. Second, mutual dependence can be due to observation preprocessing. This is so in the case of temperature and humidity retrievals from satellite measurements. Observation error correlations complicate evaluation of the cost function (2.6) and the cost function gradient (2.7) through inserting non-diagonal elements into the observation error covariance matrix. In case of ZTD observations, spatial observation error correlations are due to the geodetic processing. PAPER I focuses on the estimation of the statistical properties of the horizontal observation error covariance of ZTD.

The method applied is an extension of the observation method originally intended for background error covariance estimation (Hollingsworth and Lönnberg, 1986). The input data for the covariance estimation consists of the observation minus model background (innovation) values of ZTD, surface pressure p_s and integrated water vapour (IWV) observed at ground-based GPS receiver stations, synoptic stations and radiosonde observing stations, respectively. The dependence of ZTD on p_s and IWV is approximated as

$$ZTD \;=\; a\,p_s + b\,IWV, \tag{4.1}$$

where a = 2.2809 $\times$ 10^{-3} m hPa^{-1} and b = 6.2777. Moreover, the ZTD innovation d_{ZTD} is written as

$$d_{ZTD} \;=\; \varepsilon^o_{ZTD} - a\varepsilon^b_{p_s} - b\varepsilon^b_{IWV}, \tag{4.2}$$

where ε^o_{ZTD} is the ZTD observation error, and $\varepsilon^b_{p_s}$ and ε^b_{IWV} are the background errors of p_s and IWV, respectively. It is assumed that ε^o_{ZTD}, $\varepsilon^b_{p_s}$, and ε^b_{IWV} are uncorre-

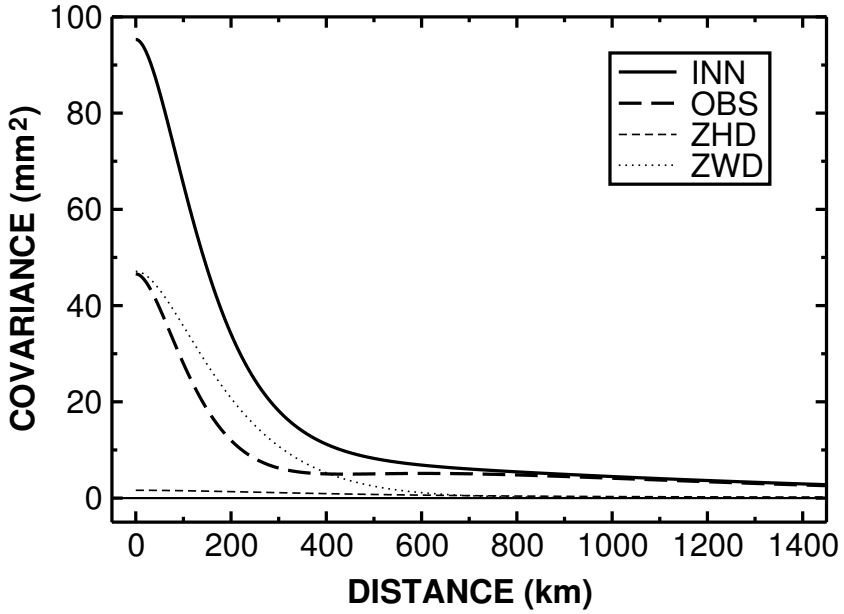

FIGURE 4.1. Terms of Eq. (4.3) as a function of station separation for the three-month autumn period (Figure 4 of PAPER I).

lated with each other, and that the observation errors are uncorrelated for both p_s and IWV. It is shown in PAPER I that, under these assumptions, the ZTD observation error covariance $cov(\varepsilon^o_{ZTD,i}, \varepsilon^o_{ZTD,j})$ and the innovation covariances are related through

$$\begin{aligned} \underbrace{cov(d_{ZTD,i}, d_{ZTD,j})}_{INN-term} &= \underbrace{cov(\varepsilon^o_{ZTD,i}, \varepsilon^o_{ZTD,j})}_{OBS-term} \\ &+ \underbrace{a^2 cov(d_{p_s,i}, d_{p_s,j})}_{ZHD-term} + \underbrace{b^2 cov(d_{IWV,i}, d_{IWV,j})}_{ZWD-term}, \end{aligned} \tag{4.3}$$

where $cov(d_{ZTD,i}, d_{ZTD,j})$, $cov(d_{p_s,i}, d_{p_s,j})$, and $cov(d_{IWV,i}, d_{IWV,j})$ are the innovation covariances of ZTD, p_s and IWV, respectively.

The mean values of the innovation covariances are determined from the innovation data for bins of 100 km of station separation, and an isotropic covariance model

$$f(r) = R_1 \left(1 + \frac{r}{L_1}\right) exp\left(-\frac{r}{L_1}\right) + R_2 \left(1 + \frac{r}{L_2}\right) exp\left(-\frac{r}{L_2}\right), \tag{4.4}$$

is fitted to the mean values. In Eq. (4.4), r is the station separation, and R_1, L_1, R_2, and L_2 are the model parameters. Figure 4.1 shows the fitted innovation covariance models (INN, ZHD and ZWD -terms) as a function of station separation for the autumn season. The heavy dashed line represents the ZTD observation error covariance determined as a linear combination of the three innovation covariance models. The conclusions from Fig. 4.1 are as follows:

- At station separations shorter than 400 km, the IWV background error covariance (ZWD -term; dotted line in Fig. 4.1) is the main contributor to the ZTD

innovation covariance.

- The ZTD observation error covariance (heavy dashed line in Fig. 4.1) appears relatively large at station separations shorter than 200 km.
- At station separations longer than 700 km, the ZTD observation error covariance equals the ZTD innovation covariance (solid line in Fig. 4.1).
- The surface pressure innovation covariance (ZHD -term; thin dashed line in Fig. 4.1) contributes very little to the ZTD innovation covariance.

Finally, the ZTD observation error covariance is approximated by the isotropic covariance model (Eq. (4.4)). This approximation is obtained by using two slightly different estimation methods. First, the 12 -parameter covariance model, resulting from the linear combination of the three four-parameter innovation covariance models, is used as input for a least-squares fitting in order to obtain a single four-parameter model. This method is called "estimation in model space". Second, the ZTD observation error covariances are calculated directly from the bin-averaged innovation covariances, and the least-squares fitting of Eq. (4.4) is performed only once. This method is called "estimation in innovation space".

The covariance model parameters are determined separately for each season and for the yearly mean. The resulting ZTD observation error covariance parameters are shown in Table 4.1. The results of the two estimation methods generally support each other, in particular in the case of the yearly mean parameters. The seasonal values show considerable differences, which effectively appear in the covariance models at very short station separations. These differences are likely to be due to the insufficient horizontal resolution of the radiosonde observing network (Stoew et al., 2001).

Table 4.1 Seasonal and yearly mean parameters of the ZTD observation error covariance model. For each season, the upper row represents "estimation in model space", and the lower row represents "estimation in innovation space".

	R_1 (mm^2)	L_1 (km)	R_2 (mm^2)	L_2 (km)
Spring	36.1	34.1	21.2	218
	90.6	23.0	22.5	214
Summer	105	56.0	14.4	237
	175	34.8	28.7	168
Autumn	41.9	61.0	5.71	813
	72.9	45.8	4.92	1730
Winter	36.1	46.1	13.3	833
	29.2	55.5	12.5	870
Yearly mean	60.0	61.4	9.97	423
	61.0	62.3	9.19	476

4.2 SLANT DELAY OBSERVATION OPERATOR

PAPER II deals with the development and validation of an observation operator for Slant Delay observations. Equations (3.4) and (3.5) shown in Section 3 provide the basis for the observation operator development. In principle, the SD observation operator reduces to a numerical integration of the refractivity along the signal path across the model atmosphere. In practice, the task of SD observation modelling is considerably more difficult, since the signal path needs to be determined as a part of the observation operator. The approach taken in PAPER II is to treat the signal path as a straight geometric line, as a first approximation. This approximation provides the concept of Geometrical Path (GP), which is further modified by adding an explicit correction in order to take the refractive bending into account. Ray-tracing based on Fermat's principle of least travel time would provide an alternative approach, in which the effect of refractive bending would be implicitly accounted for (Rodgers, 2000).

The SD observation operator determines the signal path across the model grid, interpolates the model variables from the model grid onto the signal path, calculates the refractivity distribution along the signal path, and integrates the refractivity along the signal path.

Two approaches are introduced for the validation of the observation operator. First, the sensitivity of the modelled SD to the vertical discretization of the NWP model is studied. Table 4.2 shows the SD for GPS satellites at zenith angles of 0° and 80°, corresponding to the sub-arctic summer reference atmosphere discretized at 31, 61, 121, 241, 481, 961 and 1921 levels. In principle, the observation operator should show no dependence on the details of the model discretization. According to Table 4.2, the dependence in this case is below the level of 0.1 cm of SD. Comparison, for instance, with the standard deviation of SD observation minus background -departure (Fig. 5b in PAPER II) shows that such a dependence is negligible with respect to the other inaccuracies present in SD modelling.

The second approach for the validation is based on comparing the modelled SD

Table 4.2 Slant Delay, in centimetres, in a reference atmosphere at satellite zenith angles of 0° and 80° as a function of the number of NWP model levels (K) (Table 2 of PAPER II).

K	SD 0°	SD 80°
31	242.98	1346.64
61	242.95	1346.56
121	242.95	1346.57
241	242.95	1346.57
481	242.95	1346.57
961	242.95	1346.57
1921	242.95	1346.55

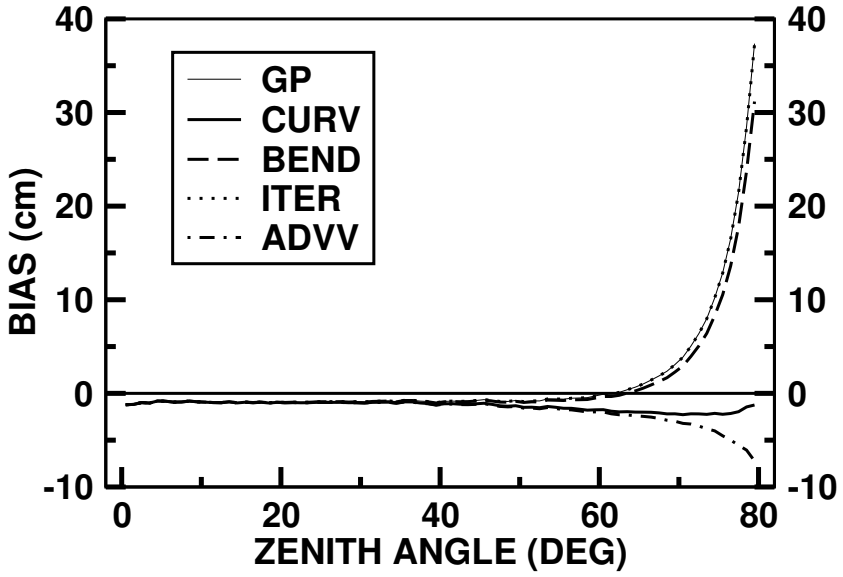

FIGURE 4.2. Mean of the difference between modelled and observed SD as a function of satellite zenith angle as calculated using different observation operator versions (Figure 5a of PAPER II).

with the SD observations. The data set used consists of 360 857 SD observations processed at the Technical University of Delft for 16 receiver stations located in the Netherlands, Belgium, Germany, Great Britain and Sweden. The data set spans the time period of 1–24 May 2003.

Three simplifications of the SD modelling are studied. These simplifications neglect (1) the apparent decrease of the satellite zenith angle (due to Earth's curvature) as the viewing point moves along the signal path towards the satellite, (2) the apparent decrease of the satellite zenith angle due to refractive bending of the signal path, and (3) the effect of the NWP model level height gradients on signal path determination. The impacts of these simplifications are illustrated in Fig. 4.2. Each curve refers to one observation operator version and shows the mean difference between the modelled and the observed SD as a function of satellite zenith angle. While the ADVV version of the observation operator (dash-dotted line) applies no simplifications and is the most advanced observation operator utilized in this study, the GP version (thin solid line) applies all three simplifications. The other versions differ from GP by applying only two of the three possible simplifications. The differences (CURV-GP), (BEND-GP) and (ITER-GP) therefore show the impacts of taking into account the decrease of zenith angle due to Earth's curvature, the decrease of zenith angle due to refractive bending of the signal path, and the effect of the NWP model level height gradients, respectively.

Figure 4.2 shows no difference between the GP and ITER curves. It is concluded that the model level height gradients can be neglected, at least in the cases represented by the verifying SD data set. On the other hand, the effects of refractive bending and the

Earth's curvature on the apparent satellite zenith angle seem to be too large to warrant being neglected by the observation operator. This conclusion holds in particular at satellite zenith angles larger than about 60°.

Figure 4.2 suggests that the SD data assimilation would benefit from the implementation of a bias correction algorithm, in particular at large satellite zenith angles. However, it is possible that modelling improvements may eliminate the need for the bias correction in the future. One potential improvement would include the effect of geometric delay, i.e., the increase of the signal path length that is due to refractive bending, in the SD modelling. It is obvious that such an improvement in the observation operator would result in a shift of the ADVV curve towards zero at zenith angles 70°–80°.

4.3 Data assimilation issues for slant delay observations

Paper III describes further developments made in order to enable the data assimilation of SD observations in the HIRLAM 3D-Var framework. These tasks include writing the tangent-linear and adjoint codes for the non-linear observation operator, implementation of the observation operator in the data assimilation architecture, determination of the observation error statistics, tuning of the observation quality control parameters, and modifying the data assimilation code in order to enable accounting for the local observation error correlation. Moreover, the impact of the SD data assimilation on the numerical analyses is validated by experiments using hypothetical observations, and the impact of real SD data is compared with impacts from other humidity observation types.

Figure 4.3 plots the vertical profile of the specific humidity analysis increment (solid line) in the case of assimilating a hypothetical SD observation at a satellite zenith angle of 0°. For comparison, the background specific humidity profile is also plotted (dashed line). It is noteworthy that, even though most of the background water vapour is below the pressure level of 925 hPa, the largest analysis increment occurs higher in the atmosphere. In fact, the vertical structure of the analysis increment is determined solely by the specification of the specific humidity background error variances. This follows from the SD observation being an integral measure of refractivity. Earlier studies have shown that the uncertainty in the background humidity is largest at pressure levels close to 800 hPa (Andersson et al., 2000; Berre, 2000).

An experiment is conducted in order to demonstrate the capability of the data assimilation system to extract the azimuthally-asymmetric information content from the SD observations. The experiment consists of assimilating eight hypothetical SD observations from a single ground-based receiver station. The characteristics of the observations are tuned corresponding to the hypothesis of a zonal gradient in the specific humidity background error at the receiver station. Figure 4.4 shows the resulting analysis increment in specific humidity at a single NWP model level. The analysis increment

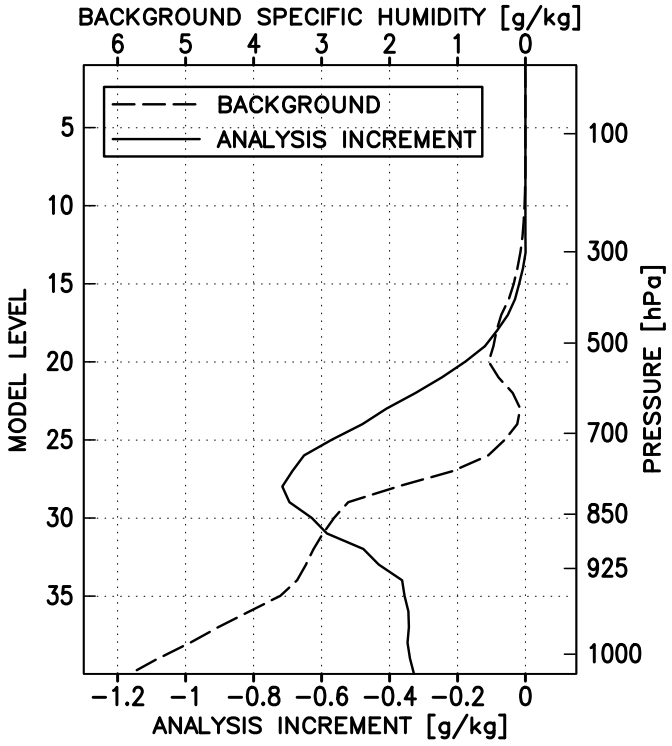

FIGURE 4.3. Vertical profiles of the background (dashed line) and the analysis increment (solid line) of specific humidity (Figure 3 of PAPER III).

is clearly asymmetric, showing maximum absolute increments shifted by about 200 km to the west and to the east of the receiver station. In a 3D-Var context, such a dipole structure could not be obtained by assimilating, for instance, ZTD observations from a single receiver station. The horizontal spread of the analysis increment follows from the specification of the specific humidity background error covariances.

4.4 ASYMMETRY PROPERTIES OF SLANT DELAY

The azimuthally-asymmetric properties of both SD observations and their NWP model counterparts are investigated in PAPER IV. There the hypothesis is stated that the SD observations contain information on atmospheric asymmetry. The paper aims at demonstrating the validity of this hypothesis. Such a demonstration is considered to be crucial for the motivation of SD data assimilation: if the hypothesis were not found to be valid, no reason would exist to believe that the SD observations could provide information which was not provided by the ZTD observations. Moreover, in order to justify SD data assimilation, the NWP model grid is required to be dense enough, so that the meteorological phenomena represented by the asymmetric information can, at least partly, be modelled explicitly.

The study makes use of SD observations and their NWP model counterparts as

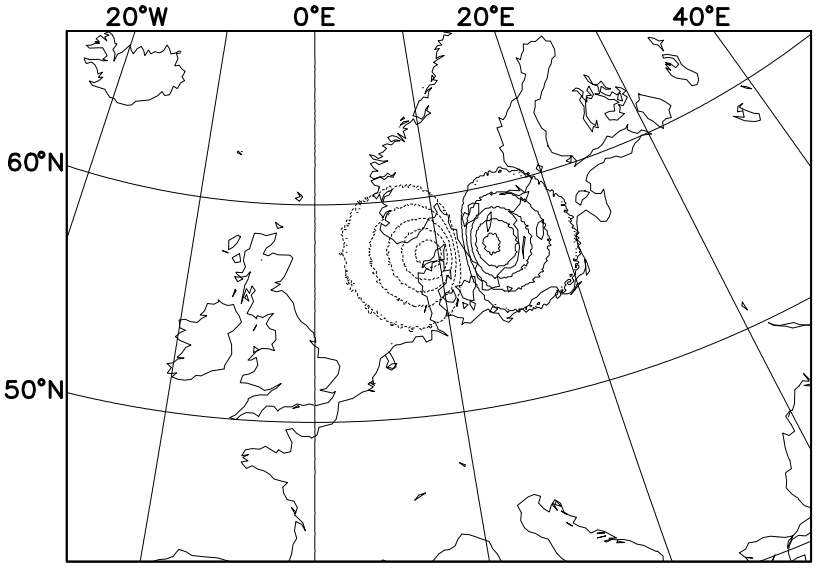

FIGURE 4.4. Specifi c humidity analysis increment on model level 27 (at approximately 770 hPa) resulting from the data assimilation of eight hypothetical SD observations observed at a single receiver station (at 57.40°N, 11.93°E). Contour interval is 0.02 g kg^{-1}, negative contours are dashed and the zero contour is omitted (Figure 6 of PAPER III).

calculated from three-hour forecasts of the HIRLAM model run at four different horizontal resolutions. For an observation or a model counterpart SD_i, the asymmetric component $SD_{a,i}$ is obtained through

$$SD_{a,i} \;=\; SD_i - m_h \left[\frac{1}{M} \sum_{i=1}^{M} \frac{SD_i}{m_i} \right], \tag{4.5}$$

where m_h is the hydrostatic mapping function proposed by Niell (1996), and M is the number of simultaneous SD observations at the receiver station in question. Effectively, this procedure first determines the symmetric component SD_s (second term on the right-hand-side of Eq. (4.5)), which is then subtracted from the total SD. As all of the SD components are very highly dependent on the satellite zenith angle, a concept of asymmetricity is introduced in PAPER IV as

$$r_a \;=\; \frac{|\mathrm{SD}_a|}{\mathrm{SD}}. \tag{4.6}$$

Figure 4.5 shows the percentages of those SD observations and NWP model counterparts, which exceed a given threshold of asymmetricity. The percentage curves are plotted for the NWP grid spacings of 22, 11, 5.6, and 2.8 km. Figure 4.5 gives an idea of the typical magnitude of the asymmetric contribution in SD; it turns out that this contribution is usually of the order of 1–3 parts per thousand (ppt), while in extreme cases it can reach 5–7 ppt of the total SD.

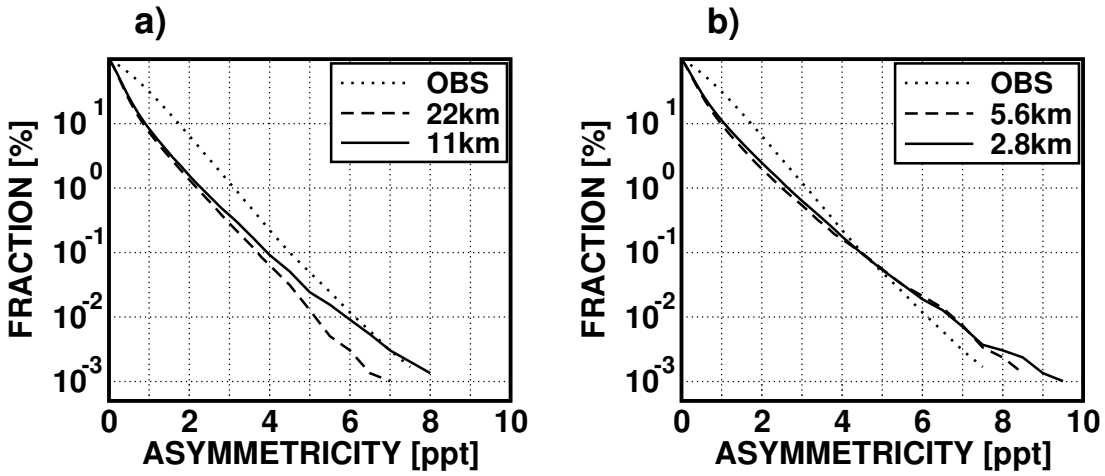

FIGURE 4.5. Percentages of SD observations and NWP model counterparts that exceed a given threshold of asymmetricity. (a) Observations (dotted) and model counterparts calculated with grid spacings of 22 km (dashed) and 11 km (solid). (b) As (a), but for model counterparts calculated with grid spacings of 5.6 km (dashed) and 2.8 km (solid) (Figures 2 and 3 of PAPER IV).

The behaviour of the observed and the modelled percentage curves are quite different. Cases in which the observed asymmetricity is smaller than 3 ppt constitute about 99% of all cases. If only these cases are concerned, all NWP model resolutions fail to represent the asymmetricity of observations (dotted line in Fig. 4.5). On the one hand this suggests that the SD observations contain spurious asymmetricity during periods of a symmetric atmosphere. This could be understood as the effect of GPS measurement noise. On the other hand, it is possible that the small asymmetricity values are mainly related to those small-scale atmospheric phenomena that cannot be resolved with the NWP models used in this study. In cases of larger asymmetricity, i.e., r_a between 3 and 5 ppt, it appears that densifying the model grid improves the representation of the asymmetricity. The percentages of asymmetricities larger than 5 ppt are overestimated at grid spacings of 5.6 and 2.8 km (Fig. 4.5b). One reason for this overestimation could be that part of the asymmetricity contained in the raw data is lost during SD data processing.

Figure 4.5b shows that a grid spacing of 5.6 km performs as well as one of 2.8 km in terms of modelling the asymmetricity. In contrast, the histograms of the asymmetric delay component at limited satellite zenith angle intervals suggest that this conclusion holds only for cases in which the satellite zenith angle is larger than 65° (see Figs. 4 and 5 of PAPER IV). At smaller zenith angles, the 2.8 km grid spacing outperforms all of the other studied model resolutions. Since the asymmetricity appears most evidently at the large zenith angles, it is concluded that extraction of the asymmetric information content of the SD observations requires a horizontal resolution of around 5 km or less in the NWP system.

5 CONCLUSIONS

Ground-based GPS meteorology provides observations of tropospheric delay, which is an integral of the neutral refractivity along either the local vertical (ZTD observations) or the actual signal path from the satellite to the receiver (SD observations). This thesis describes the methodological development carried out in order to improve the capability of the HIRLAM NWP system to make use of ground-based observations using the GPS system. The development issues presented are relevant for data assimilation of both ZTD and SD observations.

The ZTD and SD observations are obtained from the processing of raw GPS measurement data through a geodetic network solution. This processing methodology implies mutually dependent observations, with spatially and temporally correlated observation errors. These error correlations need to be taken into account in order to maintain the statistical optimality of the data assimilation. As shown in PAPER I, the spatial ZTD observation error covariance can be estimated by an extended observation method. This method uses time sequences of observation minus model background (OmB) -departures of surface pressure, integrated water vapour and ZTD, corresponding to the observations from the synoptic stations, radisonde stations and ground-based GPS receiver stations, respectively. The ZTD observation errors turn out to be correlated on spatial scales extending up to several hundreds of kilometres. However, the correlation is most significant on scales shorter than about 200 km. Since the applicability of the extended observation method is limited by the sparse resolution of the radiosonde observing network, the need for alternative estimation methods remains. For instance, ensemble data assimilation algorithms provide a promising alternative to the extended observation method. The temporal error covariance of ZTD observations has not been studied in this thesis.

SD observations possess the inherent characteristic of containing information about the azimuthal asymmetries of the atmospheric refractivity field in the vicinity of a single GPS receiver station. This asymmetry property makes this observation type a particularly interesting alternative to ZTD observations. The results presented in PAPER IV suggest that the asymmetric information content is of significance in convective-scale data assimilation, where the grid spacing is not larger than about 5 km. NWP models with coarser grids are incapable of representing the azimuthal asymmetry of SD observations. In the case of synoptic-scale data assimilation, ZTD observations are therefore expected to have the potential for providing just as complete a description of atmospheric humidity in three dimensions, as that provided by SD observations.

Observation modelling constitutes an essential part of data assimilation. PAPER II focuses on the modelling of SD observations and presents an observation operator that is based on a straight-line approximation of the signal path. The effect of refractive bending is taken into account by an explicit correction. Statistical verification indicates a systematic difference between the observed and the modelled SD, in particular

at large satellite zenith angles. Despite the fact that it is not clear whether the systematic difference is mainly due to observation or modelling errors, it is obvious that the observation operator could be improved by further modifications. One potential improvement would allow accounting for the effect of geometric delay, i.e., the increase of the signal path length due to refractive bending.

Finally, the data assimilation of SD has been shown to have the potential to extract asymmetric information content from the observations for insertion into the numerical analysis (PAPER III). More experiments still need to be conducted in order to see whether this property plays a role in the data assimilation of real SD observations. The implementation of a variational convective-scale data assimilation system is considered to be a prerequisite for these experiments.

REFERENCES

Alber, C, Ware, R, Rocken, C and J Braun, 2000: Obtaining single path phase delays from GPS double differences. *Geophys. Res. Lett*, **27**, 2661–2664.

Andersson, E, Fisher, M, Munro, R and A McNally, 2000: Diagnosis of background errors for radiances and other observable quantities in a variational data assimilation scheme, and the explanation of a case of poor convergence. *Q. J. R. Meteorol. Soc.*, **126**, 1455–1472.

Andersson, E, Pailleux, J, Thépaut, J-N, Eyre, J R, McNally, A P, Kelly, G A and P Courtier, 1994: Use of cloud-cleared radiances in three/four-dimensional variational data assimilation. *Q. J. R. Meteorol. Soc.*, **120**, 627–653.

Berre, L, 2000: Estimation of synoptic and mesoscale forecast error covariances in a limited-area model. *Mon. Wea. Rev.*, **128**, 644–667.

Bevis, M, Businger, S, Herring, T A, Rocken, C, Anthes, R A and R H Ware, 1992: GPS meteorology: Remote sensing of atmospheric water vapor using the Global Positioning System. *J. Geophys. Res.*, **97**, 15787–15801.

Bevis, M, Businger, S, Chiswell, S, Herring, T A, Anthes, R A, Rocken, C and R H Ware, 1994: GPS meteorology: Mapping zenith wet delays onto precipitable water. *J. Appl. Meteor.*, **33**, 379–386.

Blewitt, G, 1997: Basics of the GPS technique: observation equations. pp. 9–54 in Geodetic applications of GPS, edited by B Jonsson. National Land Survey of Sweden.

Boehm, J and H Schuh, 2004: Vienna mapping functions in VLBI analyses. *Geophys. Res. Lett.*, **31**, L01603, doi: 10.1029/2003GL018984.

Boehm, J, Niell, A, Tregoning, P and H Schuh, 2006, Global Mapping Function (GMF): A new empirical mapping function based on numerical weather model data. *Geophys. Res. Lett.*, **33**, L07304, doi:10.1029/2005GL025546.

Courtier, P, Thépaut, J-N and A Hollingsworth, 1994: A strategy for operational implementation of 4D-Var, using an incremental approach. *Q. J. R. Meteorol. Soc.*, **120**, 1367–1387.

De Haan, S, van der Marel, H and S Barlag, 2002: Comparison of GPS slant delay measurements to a numerical model: case study of a cold front passage. *Phys. Chem. Earth*, **27**, 317–322.

De Haan, S, Barlag, S, Klein Baltink, H, Debie, F and H van der Marel, 2004: Synergetic use of GPS water vapor and Meteosat images for synoptic weather forecasting. *J. Appl. Meteor.*, **43**, 514–518.

De Pondeca, M and X Zou, 2001: A case study of the variational assimilation of GPS zenith delay observations into a mesoscale model. *J. Appl. Meteor.*, **40**, 1559–1576.

Derber, J and W-S Wu, 1998: The use of TOVS cloud-cleared radiances in the NCEP SSI analysis system. *Mon. Wea. Rev.*, **126**, 2287–2299.

Elgered, G, Plag, H-P, van der Marel, H, Barlag, S and J Nash (Eds.), 2005: *COST Action 716 – Exploitation of ground-based GPS for operational numerical weather prediction and climate applications.* European Union, Rep. EUR 21639, 234 pp.

Elosegui, P and J L Davis, 2003: Accuracy assessment of GPS slant-path determinations. In: GPS meteorology: Ground-based and space-borne applications, p. 1-35-1.

Evensen, G, 1994: Sequential data assimilation with a nonlinear quasi-geostrophic model using Monte Carlo methods to forecast error statistics. *J. Geophys. Res.*, **99**, 10143–10162.

Falvey, M and J Beavan, 2002: The impact of GPS precipitable water assimilation on mesoscale model retrievals of orographic rainfall during SALPEX'96. *Mon. Wea. Rev.*, **130**, 2874–2888.

Feltz, W F, Smith, W L, Howell, H B, Knuteson, R O, Woolf, H and H E Revercomb, 2003: Near-continuous profiling of temperature, moisture, and atmospheric stability using the Atmospheric Emitted Radiance Interferometer (AERI). *J. Appl. Meteor.*, **42**, 584–597.

Guerova, G, Bettems, J-M, Brockmann, E and C Matzler, 2006: Assimilation of COST 716 near-real time GPS data in the nonhydrostatic limited area model used at MeteoSwiss. *Meteorol. Atmos. Phys.*, **91**, 149–164.

Gustafsson, N, Berre, L, Hörnquist, S, Huang, X-Y, Lindskog, M, Navascués, B, Mogensen, K S and S Thorsteinsson, 2001: Three-dimensional variational data assimilation for a limited area model. Part I: General formulation and the background error constraint. *Tellus*, **53A**, 425–446.

Ha, S-Y, Kuo, Y-H, Guo, Y-R and G-H Lim, 2003: Variational assimilation of slant path wet delay measurements from a hypothetical ground-based GPS network. Part I: Comparison with precipitable water assimilation. *Mon. Wea. Rev.*, **131**, 2635–2655.

Hofmann-Wellenhof, B, Lichtenegger, H and J Collins, 2001: *GPS. Theory and practice*. 5th edition. Springer-Verlag. Vienna. 384 pp.

Hollingsworth, A and P Lönnberg, 1986: The statistical structure of short-range forecast errors as determined from radiosonde data. Part I: The wind field. *Tellus*, **38A**, 111–136.

Holton, J, 1992: *An introduction to dynamic meteorology*. 3rd edition. Academic Press, San Diego. 511 pp.

Houtekamer, P L and H L Mitchell, 2001: A sequential ensemble kalman filter for atmospheric data assimilation. *Mon. Wea. Rev.*, **129**, 123–137.

Lindskog, M, Gustafsson, N, Navascués, B, Mogensen, K S, Huang, X-Y, Yang, X, Andræ, U, Berre, L, Thorsteinsson, S and J Rantakokko, 2001: Three-dimensional variational data assimilation for a limited area model. Part II: Observation handling and assimilation experiments. *Tellus*, **53A**, 447–468.

Liu, H and M Xue, 2006: Retrieval of moisture from slant-path water vapor observations of a hypothetical GPS network using a three-dimensional variational scheme with anisotropic background error. *Mon. Wea. Rev.*, **134**, 933–949.

Lorenc, A C, 1986: Analysis methods for numerical weather prediction. *Q. J. R. Meteorol. Soc.*, **112**, 1177–1194.

MacDonald, A E, Xie, Y and R H Ware, 2002: Diagnosis of three-dimensional water vapor using a GPS network. *Mon. Wea. Rev.*, **130**, 386–397.

McClatchey, R A, Fenn R W, Selby J E A, Volz F E and J S Garing, 1971: Optical properties of the atmosphere. Report AFCRL-71-0279, Air Force Cambridge Research Laboratories. 85 pp.

Niell, A E, 1996: Global mapping functions for the atmosphere delay at radio wavelengths. *J. Geophys. Res.*, **101**, 3227–3246.

Niell, A E, 2001: Preliminary evaluation of atmospheric mapping functions based on numerical weather models. *Phys. Chem. Earth (A)*, **26**, 475–480.

Niemelä, S and C Fortelius, 2005: Applicability of large-scale convection and condensation parameterization to meso-γ-scale HIRLAM: A case study of a convective event. *Mon. Wea. Rev.*, **133**, 2422–2435.

Pacione, R, Sciarretta, C, Faccani, C, Ferretti, R and F Vespe, 2001: GPS PW assimilation into MM5 with the nudging technique. *Phys. Chem. Earth (A)*, **26**, 481–485.

Pielke, R A, 2002: *Mesoscale meteorological modeling.* 2nd edition. Academic Press. San Diego. 676 pp.

Rodgers, C D, 2000: *Inverse methods for atmospheric sounding. Theory and practice*. World Scientific. Singapore. 238pp.

Rontu, L, 2006: A study on parametrization of orography-related momentum fluxes in a synoptic-scale NWP model. *Tellus*, **58A**, 69–81.

Stoew, B, Elgered, G and J M Johansson, 2001: An assessment of estimates of integrated water vapor from ground-based GPS data. *Meteorol. Atmos. Phys.*, **77**, 99–107.

Strang, G and K Borre, 1997: *Linear algebra, geodesy, and GPS*. Wellesley-Cambridge Press. Wellesley. 624 pp.

Undén, P, Rontu, L, Järvinen, H, and coauthors, 2002: HIRLAM-5 Scientific Documentation. Available from Hirlam-5 Project, c/o Per Undén, SMHI, S-60176, Norrköping, Sweden. 144 pp.

Vedel, H and X-Y Huang, 2004: Impact of Ground Based GPS Data on Numerical Weather Prediction. *J. Meteor. Soc. Japan*, **82**, 459–472.

Ware, R, Alber, C, Rocken, C and F Solheim, 1997: Sensing integrated water vapor along GPS ray paths. *Geophys. Res. Lett.*, **24**, 417–420.